The Astrophysical Journal Letters, 880:L3 (9pp), 2019 July 20 https://doi.org/10.3847/2041-8213/ab2b43

Acceleration of Energetic Ions in Corotating Interaction Region near 1.5 au: Evidence from MAVEN

Smitha V. Thampi[1], C. Krishnaprasad[1], P. R. Shreedevi[1,3], Tarun Kumar Pant[1], and Anil Bhardwaj[2]
[1] Space Physics Laboratory, Vikram Sarabhai Space Centre, Thiruvananthapuram, India; smitha_vt@vssc.gov.in
[2] Physical Research Laboratory, Ahmedabad, India
Received 2018 November 13; revised 2019 June 17; accepted 2019 June 20; published 2019 July 17

Abstract

The dearth of observations between 1 and 3 au limits our understanding of energetic particle acceleration processes in interplanetary space. We present first-of-their-kind observations of the energetic particle acceleration in a corotating interaction region (CIR) using data from two vantage points, 1 au (near Earth) and 1.5 au (near Mars). The CIR event of 2015 June was observed by the particle detectors aboard the *Advanced Composition Explorer* satellite as well as the Solar Energetic Particle (SEP) instrument aboard the Mars Atmosphere and Volatile EvolutioN (MAVEN) spacecraft situated near 1.5 au. We find that a CIR shock can accelerate a significant number of particles even at 1.5 au. During this event the acceleration by the shocks associated with the CIR could cause an enhancement of around two orders of magnitude in the SEP energetic ion fluxes in the ∼500 keV to 2 MeV range when the observations near 1 and 1.5 au are compared. To demonstrate the differences between SEP acceleration in CIR and other impulsive events, we show the energetic ion flux observations during an intense coronal mass ejection period in March 2015, in which case the enhanced SEP fluxes are seen even at 1 au. These observations provide evidence that CIR shock can accelerate particles in the region between Earth and Mars—that is, only within the short heliocentric distance of 0.5 au—in interplanetary space.

Key words: coronal mass ejections (CMEs) – solar wind – Sun: particle emission

1. Introduction

The existence of the continuous and supersonic solar wind predicted by Parker (1958) is a consequence of the supersonic expansion of the solar corona. Fast solar wind streams originate from coronal holes, and as they interact with the slow solar wind in front of it, corotating interaction regions (CIRs) are formed. The shocks associated with CIRs can accelerate energetic ions far beyond 1 au, and these particles stream into the inner heliosphere (Van Hollebeke et al. 1978; Mason & Sanderson 1999). Unlike in the case of coronal mass ejections (CMEs), the probability of CIR shocks forming within 1 au is only ∼30% (Jian et al. 2006), and whenever a solar energetic particle (SEP) event is observed at 1 au, particle flux enhancements associated with these CIRs at larger heliocentric distances show a higher particle flux intensity (Lario et al. 2000). The physical processes leading to the acceleration of these solar energetic particles are described in detail by Lee & Fisk (1982) and Desai & Giacalone (2016). The CIR-associated energetic particles in the inner heliosphere were examined using observations by various spacecraft from 1 au to ∼9 au (Van Hollebeke et al. 1978). However, most of the vantage points for these observations, including *Ulysses*, were beyond 3 au, except for two observations of Pioneer 11 at ∼1.5 au (Van Hollebeke et al. 1978), and a few observations in mid-1992 and late 1994 when *Ulysses* moved from ∼5 au near the ecliptic to a latitude of 80° S at ∼2.5 au (Richardson 2004). Apart from these isolated observations, most of the data points were from 1 au (Burlaga et al. 1985; Jian et al. 2006) and between 3 and 5 au (Van Hollebeke et al. 1978; Burlaga 1984; Lario et al. 2000; Crooker et al. 1999). While studying the radar absorption events at Mars caused by energetic particles impinging on the Martian ionosphere, Morgan et al. (2010) mentioned that the forward and reverse shocks associated with a CIR evolve between 0.5 and 2 au (Crooker et al. 1999) and therefore the orbit of Mars, between 1.4 and 1.7 au, is a key region to observe the acceleration of these energetic ions.

The Mars Atmosphere and Volatile EvolutioN (MAVEN) spacecraft was launched in 2013 November primarily to understand the atmospheric escape from Mars (Jakosky et al. 2015). MAVEN has a unique suite of instruments to measure the solar wind velocity, solar wind particle density, interplanetary magnetic field (IMF), solar wind electron pitch angle distributions, solar extreme ultraviolet (EUV) irradiance, and solar energetic electron and ion fluxes along with Martian ionosphere-thermosphere measurements. The SEP flux measurements from MAVEN provide a new vantage point near ∼1.5 au to study the acceleration of energetic particles by CIR- and CME-driven shocks.

In this study, we compare the SEP fluxes during the CIR event of 2015 June and CME events of 2015 March as observed near Earth (1 au) and near Mars (∼1.5 au) to understand the acceleration of the energetic particles beyond 1 au, especially for the CIR-driven event. The uniqueness of this study is that, for the first time, we have a vantage point to study the energetic particle fluxes near 1.5 au associated with CIRs. The CME events are shown to demonstrate the differences between the SEP fluxes in CIRs and other impulsive events at these vantage points. The direct measurements presented here, from these two key regions in space, help to understand the evolution of energetic particles in CIR and the changes in their spectral characteristics within short heliocentric distances.

2. Data

The energetic particle measurements at 1 au for the selected events are from the Electron Proton Alpha Monitor (EPAM)

[3] Now at School of Space and Environment, Beihang University, Beijing, People's Republic of China.

sensor on board the *Advanced Composition Explorer* (*ACE*) satellite. The EPAM provides particle fluxes in the energy range from 47 keV to 4.75 MeV, in eight channels. We have used ion fluxes measured in four channels in the energy ranges, 0.31–0.58 MeV, 0.58–1.05 MeV, 1.05–1.89 MeV, and 1.89–4.75 MeV by the Low Energy Magnetic Spectrometer of the EPAM sensor. These data are obtained from the *ACE* data center (http://www.srl.caltech.edu/ACE/ASC/level2/). The solar wind velocity, the IMF near 1 au and the *Geostationary Operational Environmental Satellite* (*GOES*) energetic particle flux variation (>10 MeV and >30 MeV) are obtained from the NASA Space Physics Data Facility (SPDF) OMNIWeb data center (https://omniweb.gsfc.nasa.gov/).

The solar wind velocity and IMF values at 1.5 au are obtained from the Solar Wind Ion Analyzer (SWIA) and Magnetometer (MAG) instruments on board the MAVEN spacecraft. The SWIA and MAG data are used to compute the upstream solar wind parameters following the method by Halekas et al. (2016). The SEP fluxes are obtained from the Solar Energetic Particle (SEP) instrument on board MAVEN. This instrument consists of two identical sensors, SEP 1 and SEP 2, each consisting of a pair of double-ended solid-state telescopes to measure 20 keV–1 MeV electrons and 20 keV–6 MeV ions in four orthogonal view directions (Larson et al. 2015). The data used in this study are the ion data in the form of energy fluxes measured by the SEP 1 sensor in the 1F direction that typically views the Parker spiral direction (Larson et al. 2015). The gaps in the SEP data are when the instrument attenuators close at altitudes below 500 km (Lee et al. 2017). These data sets from the MAVEN instruments are downloaded from the the Planetary Data System (https://pds.nasa.gov/). The level 2, version 01, revision 01 (V01_R01) data of SWIA, level 2, version 01, revision 01/02 (V01_R01/R02) data of MAG, and level 2, version 04, revision 02 (V04_R02) data of SEP are used for the analysis. The *Solar Dynamics Observatory* (*SDO*) images are taken from https://solarmonitor.org/. The ENLIL simulations during 2015 June and March are taken from ENLIL Solar Wind Prediction (http://helioweather.net/, https://iswa.ccmc.gsfc.nasa.gov/).

3. Overview of Events

A comprehensive overview of the solar cycle 24 space weather conditions observed during the first ~1.9 yr of the MAVEN science mission had been provided by Lee et al. (2017). The events described in this study are selected from Lee et al. (2017). During 2015 June–July, a number of low-latitude coronal holes appeared and generated recurrent high-speed streams. The *SDO*/Atmospheric Imaging Assembly (AIA) composite images of the Earth-facing disk of the solar corona shows a persistent low-latitude coronal hole that remains more or less similar even after a 27 day solar rotation period. The images of the coronal hole are given in Lee et al. (2017). The ENLIL predictions (see Appendix) reveal that the CIR hits Earth on 2015 June 7. The ENLIL snapshots further confirm that the same coronal hole with negative IMF polarity is rotated toward Mars and would arrive at Mars on 2015 June 22. Assuming to a first approximation that the rotation period for the coronal hole source is about 27.3 days, with Mars located at 1.56 au and in solar conjunction with Earth, the solar wind stream would arrive ~15.5 days later (half a Carrington rotation +~2.5 days to propagate from 1 au to 1.56 au) after the observation at Earth on June 7 (Lee et al. 2017). The ENLIL simulations also show that at *STEREO* location the CIR stream would hit on 2015 June 19 (see the Appendix). These simulations confirm that these streams are originated from the same coronal hole. Further, the study by Fisk & Lee (1980) reports that, typically, the high-speed stream is relatively steady in time, and the CIR and the shocks associated with it are stationary in the frame corotating with the Sun. Therefore, the energetic ions from a single CIR event can be seen for a period of 17 days and ~225° in solar longitude. Reames et al. (1997) also found clear evidence of energetic ions from CIR shocks over a vast spatial region corresponding to far more than half a solar rotation.

The end of 2015 February through early 2015 March was a period of intense space weather disturbances at Mars (Lee et al. 2017). Bright CME loops were observed in the southeast quadrant of the *Solar and Heliospheric Observatory* Large Angle and Spectrometric Coronagraph (LASCO) C2 field of view on 2015 March 6, and peak enhancements in solar wind speed, density, dynamic pressure, and IMF were observed at Mars on 2015 March 8 (Thampi et al. 2018, and references therein). The solar source for these events, Active Region 12297, was on the backside of the Sun (as viewed from Earth), which rotated over the east solar limb and produced a M8.9 class flare that was observed by both MAVEN and *GOES* on 2015 March 7 (Lee et al. 2017). As this active region rotated toward the direction of Earth, it produced a number of flares and CMEs including the 2015 March 17 superstorm at Earth, popularly known as the "St. Patrick's Day Storm." ENLIL simulations confirm the CME arrivals and show that these events at Earth and Mars are produced by different eruptions from the same active region (see the Appendix).

4. Observations

Figure 1(a) shows the variation of IMF and solar wind velocity as observed near 1 au during 2015 June 5–17. The CIR reached the vicinity of Earth on 2015 June 7, marked by an enhancement in velocity. This enhancement in velocity continued to remain near the highest value almost for 4 days and then remained at a slightly lower value (which is still higher than the velocities observed during 2015 June 5–7) until 2015 June 17. The *Z*-component of the IMF showed largest fluctuations on June 7 and 8, followed by fluctuations of smaller magnitude, a typical feature of a CIR-driven storm (Borovsky & Denton 2006). Figure 1(b) shows the variation of the energetic particle fluxes of energy range from ~300 keV to ~4.7 MeV as observed by the EPAM sensor on board *ACE* satellite located near 1 au. The signature of the CIR arrival is seen as ~2 orders of magnitude increase in the SEP fluxes. The arrival of the CIR is preceded by a calm period with almost no SEP fluxes. This is another typical feature of CIR events (Borovsky & Denton 2006). The flux of particles in the energy range ~0.3 MeV to ~0.5 MeV increased to >100 particles $cm^{-2}\,s^{-1}\,sr^{-1}\,MeV^{-1}$, whereas the particle flux with energies ⩾1 MeV remained ⩽10 particles $cm^{-2}\,s^{-1}\,sr^{-1}\,MeV^{-1}$.

Figure 2(a) shows the variation of IMF and solar wind velocity as observed by the MAG and SWIA instruments aboard MAVEN located at 1.56 au. The total magnetic field increased to ~9 nT coincident to the arrival of CIR. The solar wind velocity increased from the quiescent value of ~300 to

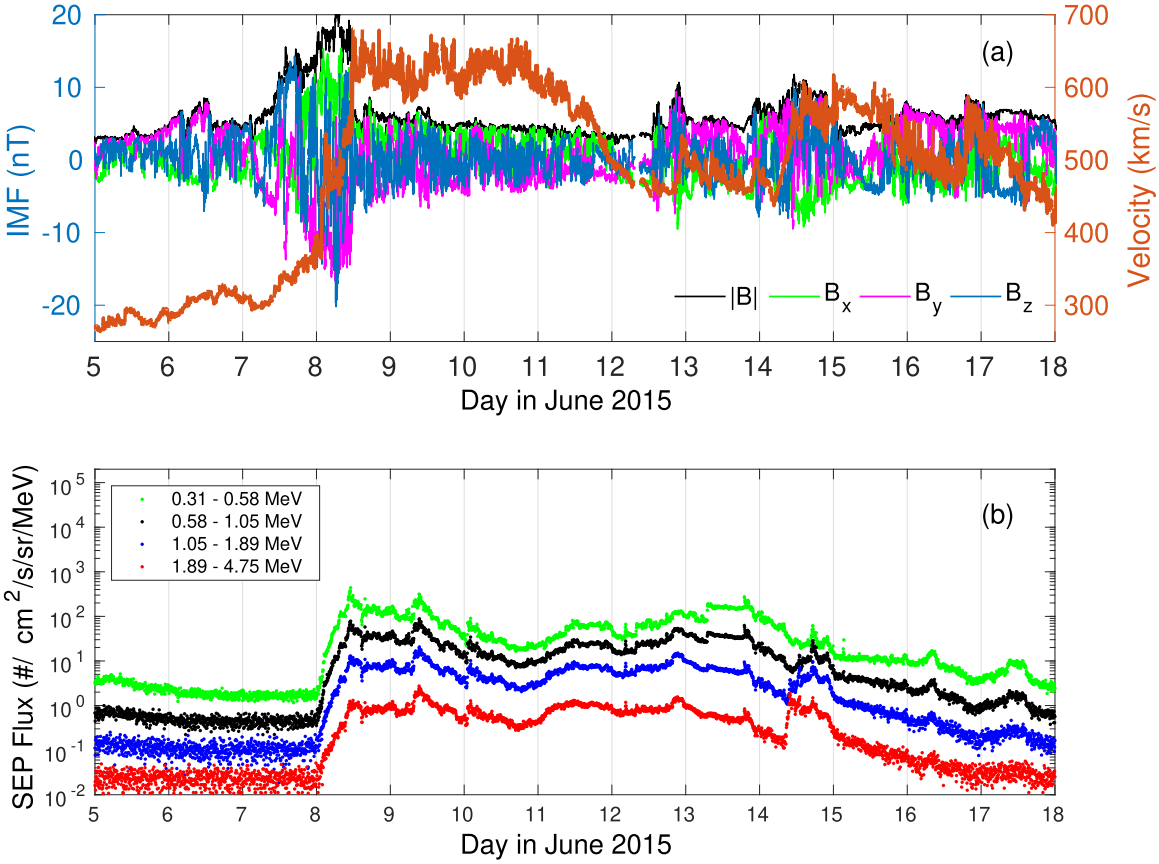

Figure 1. (a) Variation of IMF (left *Y*-axis) and solar wind velocity (right *Y*-axis) for the period 2015 June 5–17 observed by *ACE* at 1 au. (b) The SEP particle fluxes at different energy ranges as observed by the EPAM sensor on board the *ACE* satellite for the period 2015 June 5–17.

$\sim$700 km s^{-1} and remained to be $>$600 km s^{-1} for the next day as well and remained high until the end of June (Lee et al. 2017).

Figure 2(b) shows the differential energy flux spectrum of the solar energetic ions observed by the MAVEN SEP instrument. During the CIR event (on 2015 June 22 and 23), there is an enhancement in the flux of energetic particles. In order to see the actual number of accelerated energetic ions using the MAVEN SEP instrument and compare them with the observations at 1 au by *ACE*, we estimated the integrated flux at energy bins comparable to that of the EPAM/*ACE* observations (Figure 2(c)). The onset of disturbed fluxes from June 8 at Earth shown in Figure 1(b) (coinciding with the enhancements in velocity and magnetic field) correspond to the enhancement seen from June 22 to 23 at Mars in Figure 2(c). The time differences seen in the SEP enhancement at these locations is consistent with the estimated arrival time based on the solar rotation period for the coronal hole source. It must be noted that the SEP fluxes before June 19 at Mars had very low values and the source of the slightly enhanced SEPs seen on June 19–20 could be related to the streaming particles from field lines connected to a CME that erupted over the west solar limb, although the CME has not directly hit Mars (Lee et al. 2017). The SEP fluxes return to lower values (below 100 particles cm^{-2} s^{-1} sr^{-1} MeV^{-1}) before the arrival of CIR on June 22. The arrival of the CIR is marked by enhancements in solar wind velocity and magnetic field, and coincident enhancement in SEP fluxes by more than two orders from the pre-CIR levels. In comparison to the observations from 1 au, fluxes enhanced in the similar energy ranges at 1.5 au. The peak ion flux in the $\sim$1–2 MeV bin enhanced by $\sim$300 times at 1.5 au. This indicates that acceleration took place beyond 1 au, but within 1.5 au. Similarly, $\sim$140 times enhancement is observed for the flux in the $\sim$600 keV–1 MeV energy bin. Therefore, we can infer that the acceleration by the shocks associated with CIR could cause an enhancement of around two orders of magnitude in the SEP fluxes when observed near 1.5 au.

Figure 3(a) shows the energy spectrum corresponding to the peak of ion flux enhancement for the CIR event on 2015 June 8 detected by *ACE*. Double power laws are fitted, one with $E^{-1.88}$ for flux below 0.2 MeV and the second one with $E^{-2.78}$ for the flux between 0.2 and 3 MeV. These spectral indices are similar to those reported by Bučík et al. (2009) for the 2007 May events. To see whether we can expect higher-energy particles at the energy ranges of *GOES*, the *ACE* spectrum is extrapolated to 30 MeV with the same power law. With this approximation itself, it can be seen that at both 10 MeV and at 30 MeV the expected flux levels are below the detection limits of *GOES* (Rodriguez et al. 2014). A double power law or a power law with exponential rollover at a few to tens of MeV has been reported in many events (e.g., Mason & Sanderson 1999). If this is the case, then the expected flux at the higher-energy ranges will be still lower than what we estimated from a simple

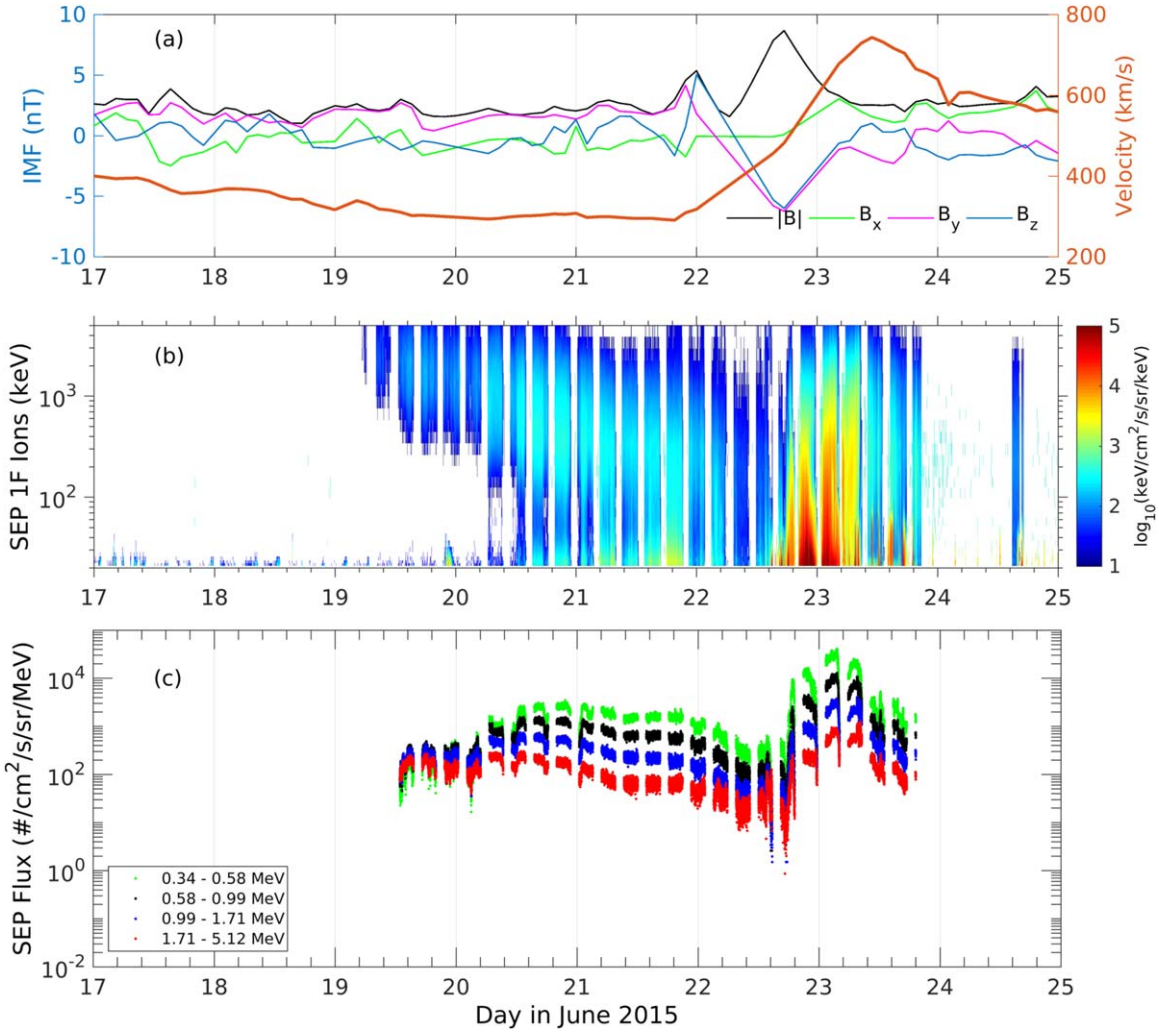

Figure 2. (a) Variation of IMF (left *Y*-axis) and solar wind velocity (right *Y*-axis) for the period 2015 June 17–24. (b) The energy spectrum of ions in the 30 KeV to ~6 MeV range observed by the MAVEN SEP instrument for the period 2015 June 17–24. The *Y*-axis shows the energy range and the color axis shows the logarithmic particle flux. The initial period shown in white had very low fluxes (<10), whereas the gaps on 2015 June 24 correspond to the absence of good quality data. (c) The integrated SEP particle fluxes in different energy ranges (comparable to *ACE* measurements) estimated from the MAVEN SEP data.

power law. Therefore, for this CIR event we do not expect that *GOES* would detect the SEP fluxes, and the observations confirm that *GOES* did not see any particles above its detection threshold.

Figure 3(b) shows the energy spectrum during peak of ion flux enhancement in the CIR event on 2015 June 23 detected by MAVEN, with power-law fits. The first portion (below 60 keV) may have contributions from the oxygen pickup ions (Larson et al. 2015). The flux in the energy range 0.5–3 MeV shows a spectral index of −2.82. At both these locations, the observed energy spectra continued to extend as power laws right down to the lowest energy measured by the instruments, which corroborates with the results of Mason et al. (1997) and Chotoo et al. (2000).

To demonstrate the difference between CIRs and other impulsive events, we show in Figure 4(a) (Figure 5(a)) the variation of IMF and solar wind velocity observed near 1 au (1.5 au), during 2015 March 5–24 (2015 March 1–13). Figure 4(a) shows that the IMF showed large fluctuations maximizing on March 17. The solar wind velocity also showed concurrent enhancement and fluctuations afterward. Figure 4(b) shows the SEP fluxes observed by the *ACE* satellite for the same period. The fluxes showed enhancement in all the energy levels during the CME event. Compared with the CIR-related energetic particle fluxes, these observations are more than two orders of magnitude higher in all the energy ranges observed by EPAM/*ACE*. This is the typical characteristic of CME-driven shock acceleration of energetic particles and one of the major difference between CME- and CIR-driven storms at 1 au. The *GOES* observations (not illustrated) also indicate the presence of particles in the >10 MeV energy range; that is, a peak flux of ~7 cm^{-2} s^{-1} sr^{-1} on March 17.

Figure 5(a) shows the variation of IMF and solar wind velocity observed by MAVEN for the period 2015 March 1–13, and Figure 5(b) shows the corresponding SEP differential energy flux spectrum. The first velocity enhancement occurred on March 3 and the highest velocity was observed on March 8. IMF variations were observed during both the events with higher magnitudes during the second event. The SEP spectrum showed flux enhancements with almost similar levels

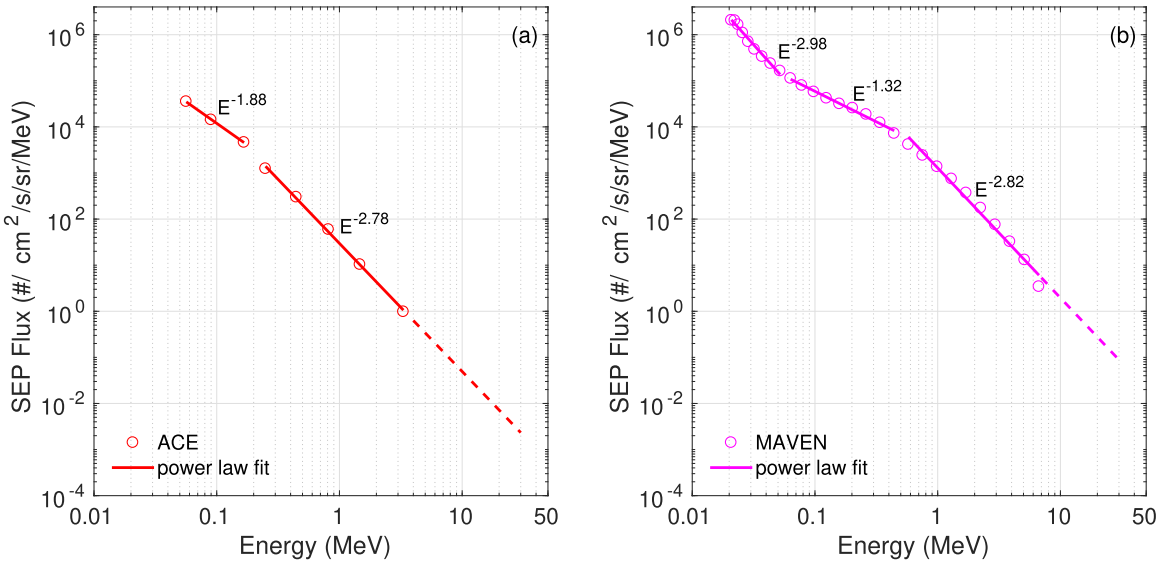

Figure 3. (a) Energy spectrum during peak of ion flux enhancement in the CIR event on 2015 June 8 detected by *ACE* at ∼1 au. The power laws fitted with the observations are also shown. The observations by *ACE* are extrapolated to 30 MeV, to show that at both 10 MeV and at 30 MeV, the expected flux levels are below the detection limits (Rodriguez et al. 2014) of *GOES*. (b) The energy spectrum obtained from MAVEN. The integration time is ∼1 hr in both energy spectra.

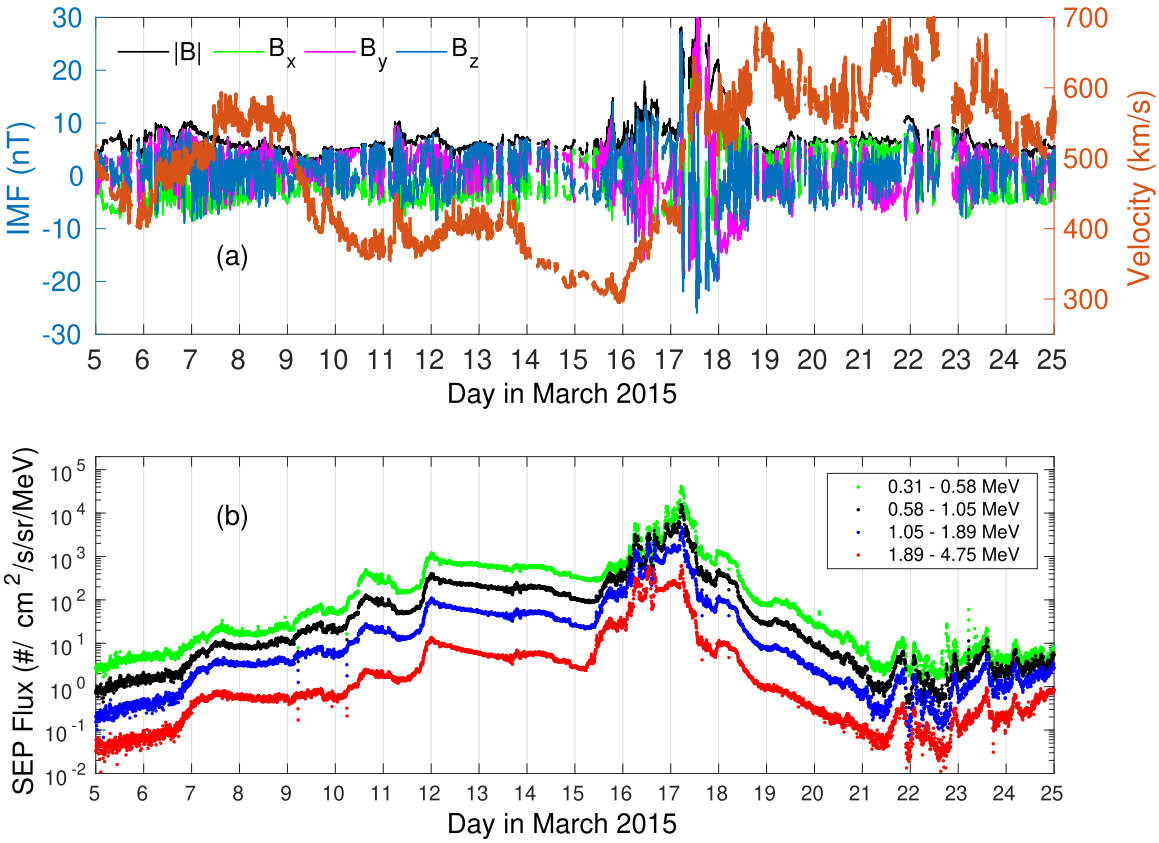

Figure 4. Same as in Figure 1, but for the period 2015 March 5–24.

on both the occasions. MAVEN observed the CME shock only after the arrival of the highest-energy SEP ions, and these high-energy (>1 MeV) ions arrived first followed by the lower-energy particles on March 7–8. Figure 5(c) shows the integrated particle fluxes at Mars in the energy ranges comparable to EPAM/*ACE*. The flux levels showed increase at ∼1.5 au at all the energy bins. In the energy range of ∼500 keV–1 MeV, the enhancement is only ∼5 times.

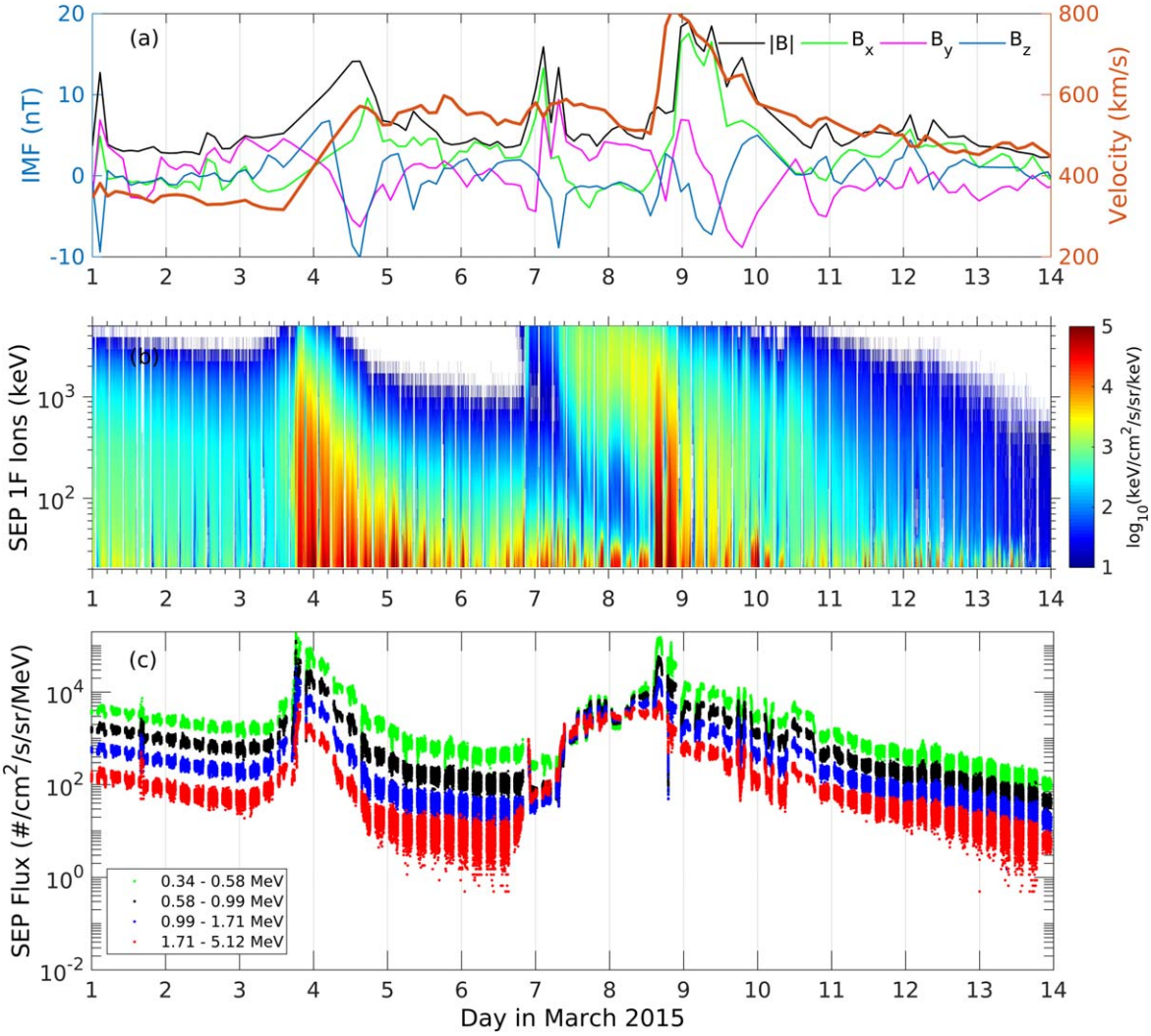

Figure 5. Same as in Figure 2, but for the period 2015 March 1–13.

5. Discussion and Conclusions

Most of the previous studies concerning CIR-driven SEP flux enhancements were confined to data from observations beyond 3 au. The radial gradient of CIR-associated energetic particle streams was measured by instruments on multiple probes to the inner heliosphere (*Helios 1* and *2*, *Mariner 10*, *Ulysses*), and the outer solar system (Pioneer 10 and 11) with reference spacecraft at 1 au such as IMP 7 and 8, *ACE*, *WIND*, and *STEREO*, and most of these measurements pertained to total ion flux in the 0.9–2.2 MeV energy range. The *Ulysses* observations at ∼1.4 au, during its rapid latitude scan phase had shown the presence of reverse waves that had not yet steepened into shocks (Gosling et al. 1995). Apart from this, there was one unambiguous observation of CIR-induced acceleration of ions near 1.5 au, by Pioneer 11, which was total ion fluxes in the energy range 0.9–2.2 MeV (Van Hollebeke et al. 1978). The enhancement in the fluxes reported here is almost an order of magnitude higher than that reported by Van Hollebeke et al. (1978).

The observations presented here clearly illustrate the following aspects.

(a) During the CME events in 2015 March, the SEP observations from both 1 and 1.5 au show enhancement of high-energy particle fluxes. The observations suggests that shock acceleration takes place at 1 au itself during CME events (Lario et al. 2000). The comparison facilitates the demonstration of the differences between SEP acceleration in CIRs and other impulsive events like CMEs.

(b) During the CIR event in 2015 June, at 1 au, *GOES* did not observe any particle flux above its detection threshold, and the particle flux $\geqslant$1 MeV detected by *ACE* remained $\leqslant$10 particles $cm^{-2}\,s^{-1}\,sr^{-1}\,MeV^{-1}$. Compared to this, the SEP instrument on board MAVEN showed high SEP fluxes up to ∼3 MeV. Comparison shows that the acceleration by the shocks associated with CIR can produce an enhancement of around two orders of magnitude in the SEP fluxes when observed near 1.5 au. Interestingly, the peak high-energy particle fluxes at Mars are of almost similar levels during a CME-driven event, indicating similar levels of acceleration during these events at 1.5 au. In contrast, these flux levels are drastically different in the case of *ACE* observations at

1 au (>one order of magnitude higher in the ~1–2 MeV range during a CME), which is consistent with the expectation that strong shock acceleration takes place inside 1 au during CME events (Li et al. 2005; Desai & Burgess 2008). The comparison of energy fluxes at different ranges may point toward the change of energy with distance as particles travel several aus in the heliosphere under cross-field diffusion (Zhao et al. 2016). These observations are unique because of the addition of a vantage point at 1.5 au, and as such observations were previously very sparse between 1 and 3 au.

The work is supported by the Indian Space Research Organisation (ISRO). The MAVEN data used in this work are taken from the Planetary Data System (https://pds.nasa.gov/). We gratefully acknowledge the MAVEN team for the data. The *ACE*/EPAM data are taken from the *ACE* Science Center (http://www.srl.caltech.edu/ACE/ASC/level2/). The solar wind velocity and IMF near 1 au, as well as the *GOES* particle flux data, are obtained from the SPDF OMNIWeb data center (https://omniweb.gsfc.nasa.gov/). We thank the staff of the *ACE* Science Center for providing the *ACE* data and NASA/GSFC OMNIWeb team for the interplanetary and *GOES* data. The WSA-ENLIL+Cone simulations are taken from ENLIL Solar Wind Prediction (http://helioweather.net/, https://iswa.ccmc.gsfc.nasa.gov/). The authors thank K. Kishore Kumar, Space Physics Laboratory, VSSC for the useful discussions on spectral analysis. The authors also thank K. Sankarasubramanian, U R Rao Satellite Centre, for the useful discussions on *SDO* solar images. C. Krishnaprasad acknowledges the financial assistance provided by ISRO through a research fellowship.

Appendix
Wang–Sheeley–Arge (WSA)-ENLIL+Cone Model Simulations

We used the WSA-ENLIL+Cone model to numerically simulate the interplanetary solar wind plasma and magnetic field conditions and provide a global heliospheric context for the solar events discussed. In this heliospheric model, the solar coronal model WSA is coupled with the three-dimensional magnetohydrodynamic numerical model ENLIL, which is combined with the Cone model (Odstrcil 2003; Mays et al. 2015).

Figures (6(a)–(d)) shows the WSA-ENLIL simulations of solar wind conditions during the CIR event on 2015 June 8 and 23 (Figures 6(a), (b)), and CME events on 2015 March 8 and 17 (Figures 6(c), (d)).

Figure 7 shows the WSA-ENLIL+Cone simulations of solar wind density and velocity during 2015 June 5–9 at Earth (Figure 7(a)) and 2015 June 18–22 at *STEREO-A* and *STEREO-B* (Figure 7(b)). Figure 7(a) shows the comparison of observations at Earth with WSA-ENLIL+Cone simulation, which show a gross agreement. We can see that the time evolution of solar wind velocity and density at Earth and *STEREO*s shows an overall similarity, which confirms that the corotating stream was relatively steady in time; that is, time stationary in the corotating frame even after half a solar rotation (Fisk & Lee 1980; Reames et al. 1997). It maybe noted here that the WSA-ENLIL+Cone simulations are used only to get a general picture of what these events might have looked like on a larger scale at 1 and 1.5 au. Though the WSA-ENLIL+Cone can provide short-term all-inclusive forecasts that are closer to the observations, the long-term forecasts may be imprecise in details (Falkenberg et al. 2011; Lentz et al. 2018). However, the predictions are reasonably accurate within 1 au (Mays et al. 2015); therefore, the simulations at *STEREO* locations (where observations are not available) are expected to be reasonable.

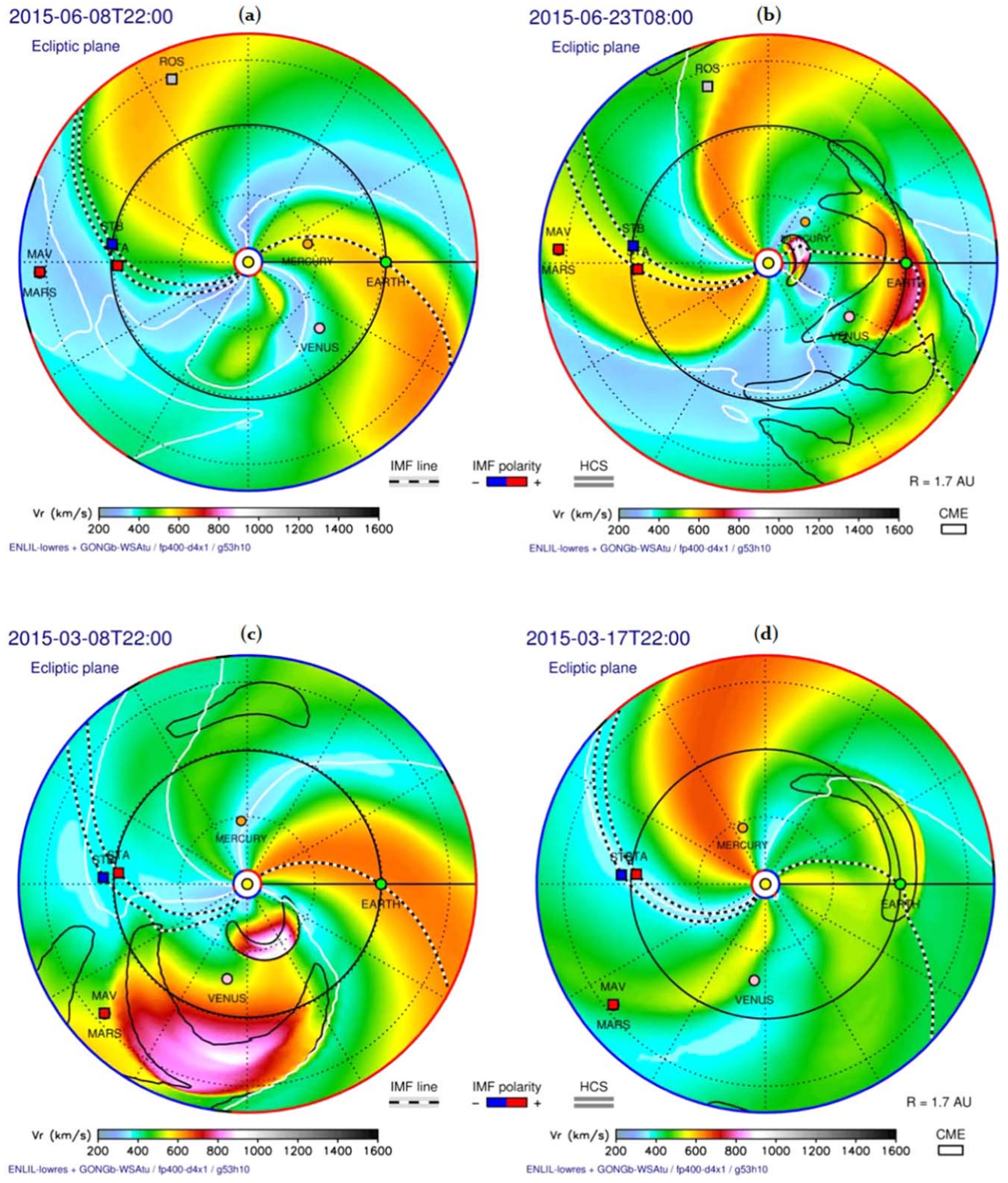

Figure 6. WSA-ENLIL simulations of solar wind during (a) 2015 June 8, (b) 2015 June 23, (c) 2015 March 8, and (d) 2015 March 17.

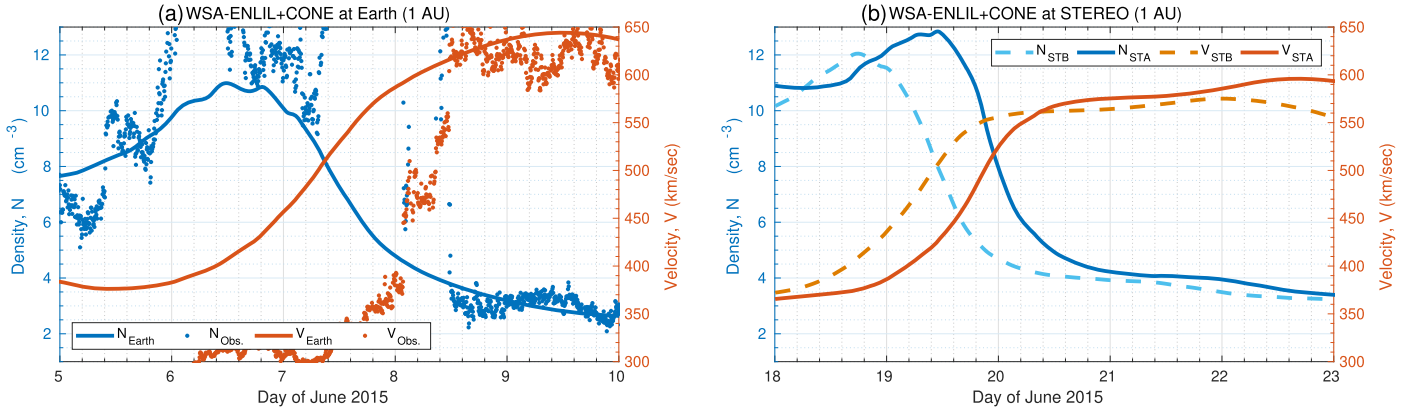

Figure 7. WSA-ENLIL+Cone simulations of solar wind density and velocity during (a) 2015 June 5–9 at Earth and (b) 2015 June 18–22 at *STEREO-A* (*STA*) and *STEREO-B* (*STB*).

ORCID iDs

Smitha V. Thampi https://orcid.org/0000-0002-0116-829X
C. Krishnaprasad https://orcid.org/0000-0002-3324-156X
P. R. Shreedevi https://orcid.org/0000-0002-0979-0833
Anil Bhardwaj https://orcid.org/0000-0003-1693-453X

References

Borovsky, J. E., & Denton, M. H. 2006, JGRA, 111, A07S08
Burlaga, L. F. 1984, SSRv, 39, 255
Bučík, R., Mall, U., Gómez-Herrero, R., Korth, A., & Mason, G. M. 2009, SoPh, 259, 361
Burlaga, L. F., Pizzo, V., Lazarus, A., & Gazis, P. 1985, JGRA, 90, 7377
Chotoo, K., Schwadron, N. A., Mason, G. M., et al. 2000, JGRA, 105, 23107
Crooker, N., Gosling, J., Bothmer, V., et al. 1999, SSRv, 89, 179
Desai, M., & Giacalone, J. 2016, LRSP, 13, 3
Desai, M. I., & Burgess, D. 2008, JGRA, 113, A00B06
Falkenberg, T. V., Taktakishvili, A., Pulkkinen, A., et al. 2011, SpWea, 9, S00E12
Fisk, L. A., & Lee, M. A. 1980, ApJ, 237, 620
Gosling, J. T., Feldman, W. C., McComas, D. J., et al. 1995, GeoRL, 22, 3333
Halekas, J. S., Ruhunusiri, S., Harada, Y., et al. 2016, JGRA, 122, 547
Jakosky, B. M., Lin, R. P., Grebowsky, J. M., et al. 2015, SSRv, 195, 3
Jian, L., Russell, C. T., Luhmann, J. G., & Skoug, R. M. 2006, SoPh, 239, 337
Lario, D., Marsden, R. G., Sanderson, T. R., et al. 2000, JGRA, 105, 18251
Larson, D. E., Lillis, R. J., Lee, C. O., et al. 2015, SSRv, 195, 153
Lee, C. O., Hara, T., Halekas, J. S., et al. 2017, JGRA, 122, 2768
Lee, M. A., & Fisk, L. A. 1982, SSRv, 32, 205
Lentz, C. L., Baker, D. N., Jaynes, A. N., et al. 2018, SpWea, 16, 157
Li, G., Zank, G. P., & Rice, W. K. M. 2005, JGRA, 110, A06104
Mason, G., & Sanderson, T. 1999, SSRv, 89, 77
Mason, G. M., Mazur, J. E., Dwyer, J. R., Reames, D. V., & von Rosenvinge, T. T. 1997, ApJL, 486, L149
Mays, M. L., Taktakishvili, A., Pulkkinen, A., et al. 2015, SoPh, 290, 1775
Morgan, D. D., Gurnett, D. A., Kirchner, D. L., et al. 2010, Icar, 206, 95
Odstrcil, D. 2003, AdSpR, 32, 497
Parker, E. N. 1958, ApJ, 128, 664
Reames, D. V., Ng, C. K., Mason, G. M., et al. 1997, GeoRL, 24, 2917
Richardson, I. G. 2004, SSRv, 111, 267
Rodriguez, J. V., Krosschell, J. C., & Green, J. C. 2014, SpWea, 12, 92
Thampi, S. V., Krishnaprasad, C., Bhardwaj, A., et al. 2018, JGRA, 123, 6917
Van Hollebeke, M. A. I., McDonald, F. B., Trainor, J. H., & Rosenvinge, T. T. 1978, JGRA, 83, 4723
Zhao, L., Li, G., Ebert, R. W., et al. 2016, JGRA, 121, 77